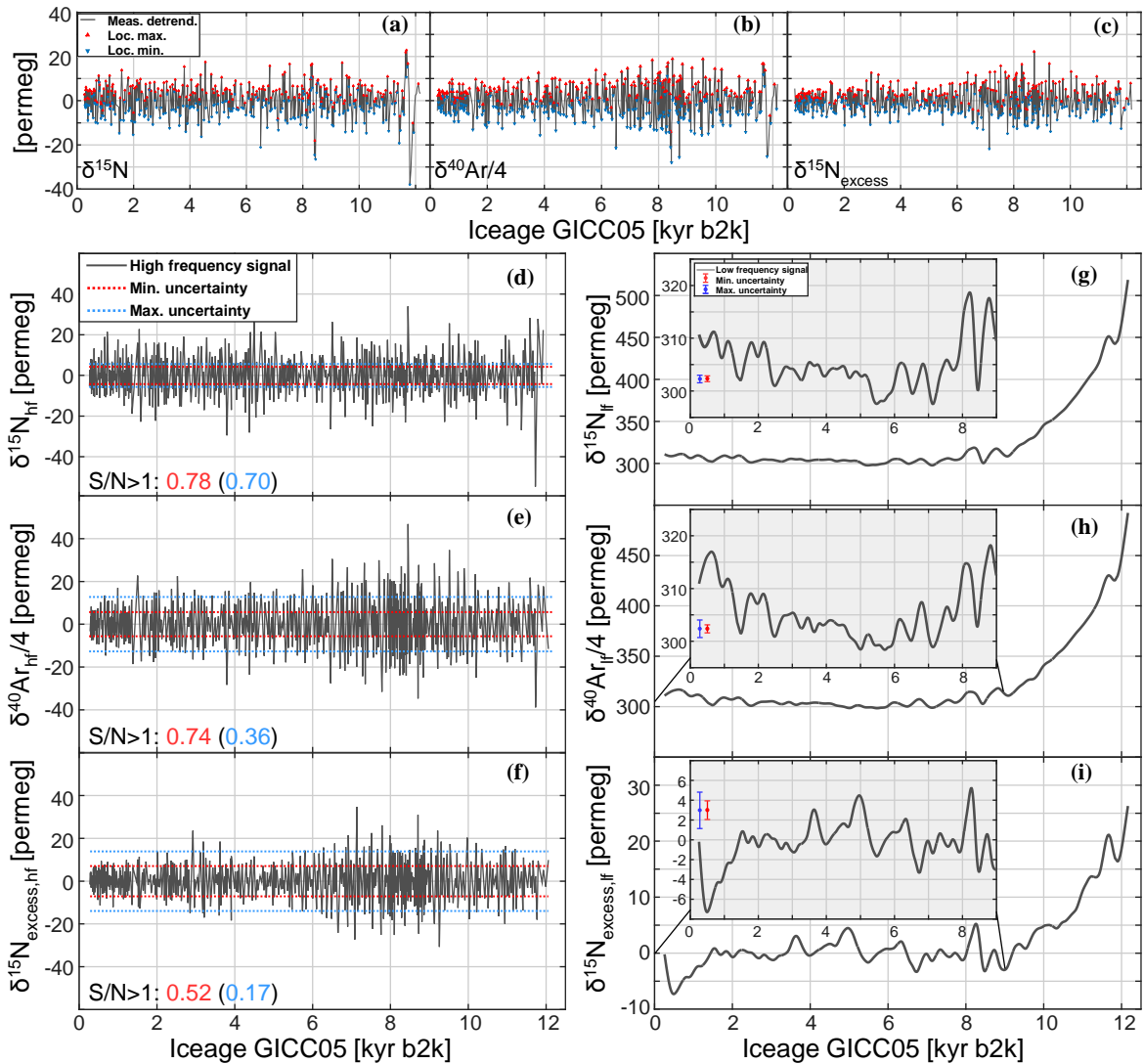


S1: Target data and their suitability

| Target: | $\delta^{15}\text{N}$ | | $\delta^{40}\text{Ar}/4$ | | $\delta^{15}\text{N}_{\text{excess}}$ | |
|---|-----------------------|------|--------------------------|------|---------------------------------------|------|
| | max | min | max | min | max | min |
| Data uncertainty 1σ [permeg]*: | 4.0 | 3.0 | 9.0 | 4.0 | 9.8 | 5.0 |
| Signal uncertainty 1σ [permeg]: | 5.7 | 4.2 | 12.7 | 5.7 | 13.9 | 7.1 |
| SNR > 1 hf-signals [%]: | 70.0 | 78.0 | 35.7 | 74.2 | 16.5 | 52.3 |

Table S1: Reported data uncertainty (*Kobashi et al., 2008b), calculated signal uncertainties (see section 2.2.: Target data and their suitability) and percentage of high frequency signals with SNR > 1.



5 **Figure S1: Signal-to-noise analysis of the used target data (data from Kobashi et al., 2008b). (a-c): Detrended**

(cop = 500 yr) $\delta^{15}\text{N}$, $\delta^{40}\text{Ar}/4$ and $\delta^{15}\text{N}_{\text{excess}}$ high-frequency data. Triangles indicate local maxima (red) and local minima (blue) used to calculate the high-frequency signals. (d-f): $\delta^{15}\text{N}$, $\delta^{40}\text{Ar}/4$ and $\delta^{15}\text{N}_{\text{excess}}$ high-frequency signals (grey line) calculated from the differences of local minima and maxima of the detrended high-frequency data and minimum (red dotted line) and maximum (blue dotted line) signal uncertainties (see text). The red and blue numbers indicate the fraction of signals with amplitudes higher than the related uncertainties. (g-i): $\delta^{15}\text{N}$, $\delta^{40}\text{Ar}/4$ and $\delta^{15}\text{N}_{\text{excess}}$ low-frequency data (cop = 500 yr) and zoom-in for the last 9 kyr together with the maximum (blue) and minimum (red) measurement uncertainty (Kobashi et al., 2008) divided by 5.3 (= (500 yr/17.8 yr)^{0.5}).

S2: Model Spin-Up

To avoid the influence of possible memory effects (influence of earlier firn-state conditions on later firn-states) on the model output of the reconstruction window, a temperature and accumulation-rate spin-up is needed in order to bring the firn-model to a well-defined starting condition. For constructing the surface temperature spin-up we use the temperature reconstruction for the GISP2 site from Buizert et al. (2014) for the interval 10.05 kyr to 20 kyr b2k. The reconstruction is based on $\delta^{18}\text{O}_{\text{ice}}$ -calibration and on $\delta^{15}\text{N}$ -fitting using a dynamical firn-densification-model. We further extend the temperature spin-up to 35 kyr b2k by calibrating the GISP2 $\delta^{18}\text{O}_{\text{ice}}$ data (Grootes et al., 1993; Grootes and Stuiver, 1997; Meese et al., 1994; Steig et al., 1994; Stuiver et al., 1995; data availability: Grootes and Stuiver, 1999) using the slopes and intercepts for the linear calibration given in Cuffey and Clow (1997). For the reconstruction window corresponding to the Holocene (0.02 kyr to 11.50 kyr b2k), we simply start with constant temperature using the last value of the spin-up section (10.05 kyr b2k, fig. S2, black line). Since we use three accumulation-rate scenarios (50 km, 100 km, 200 km) and a different firn-model as Buizert et al. (2014), it was necessary to adjust the model spin-up temperature in order match the decreasing flank at the oldest part (9.5 kyr to 12.168 kyr b2k) of the gas-isotope data. The adjustment was done for all three used accumulation-rate scenarios separately. The constant offset of about 0.05 permil (or 4 K for the temperatures) between the modelled $\delta^{15}\text{N}$ using the unadjusted prior temperature and the adjusted temperatures potentially originates from two sources. First, from the fact that the firn-model of Schwander et al. (1997) does not incorporate a convective zone and thereof a larger firn column is modelled. To model the gravitational component of the isotope fractionation, a higher absolute temperature is needed, accelerating densification and leading to a reduced firn column. Second, the Schwander et al. (1997) firn-model does not model basal heat-flow, which leads to a certain enrichment of the modelled isotopes compared to models which incorporate that quantity. The adjustment is described in the example of $\delta^{15}\text{N}$ data in the following. The temperature spin-up was divided in different sections indicated by the time markers A, B, C and D (fig. S2a). The sections [start to A], [B to C], and [D to end] were shifted with certain offsets to provide the best possible fit with the decreasing flank in the oldest part of the gas-isotope data. In-between A and B, and C and D the missing values were linearly interpolated. To find the three optimum offset parameter, Nelder-Mead simplex minimisation was used (Lagarias et al., 1998). Figure 2c shows the modelled $\delta^{15}\text{N}$ values before (black) and after the adjustment (for different accumulation-rate scenarios: blue: 50 km, red: 100 km, yellow: 200 km) together with the measured $\delta^{15}\text{N}$ data (grey). Figures 2d,e illustrates the differences between the model-outputs using the same spin-up adjustment (i.e. for 100 km acc-scenario) for all three accumulation-rate scenarios (d) and the outputs, where we conducted an individual adjustment for each scenario (e). Using the same spin-up for all three accumulation-rate scenarios leads to small but significant divergences between the model-outputs lasting for about 2 kyr (d vs. e).

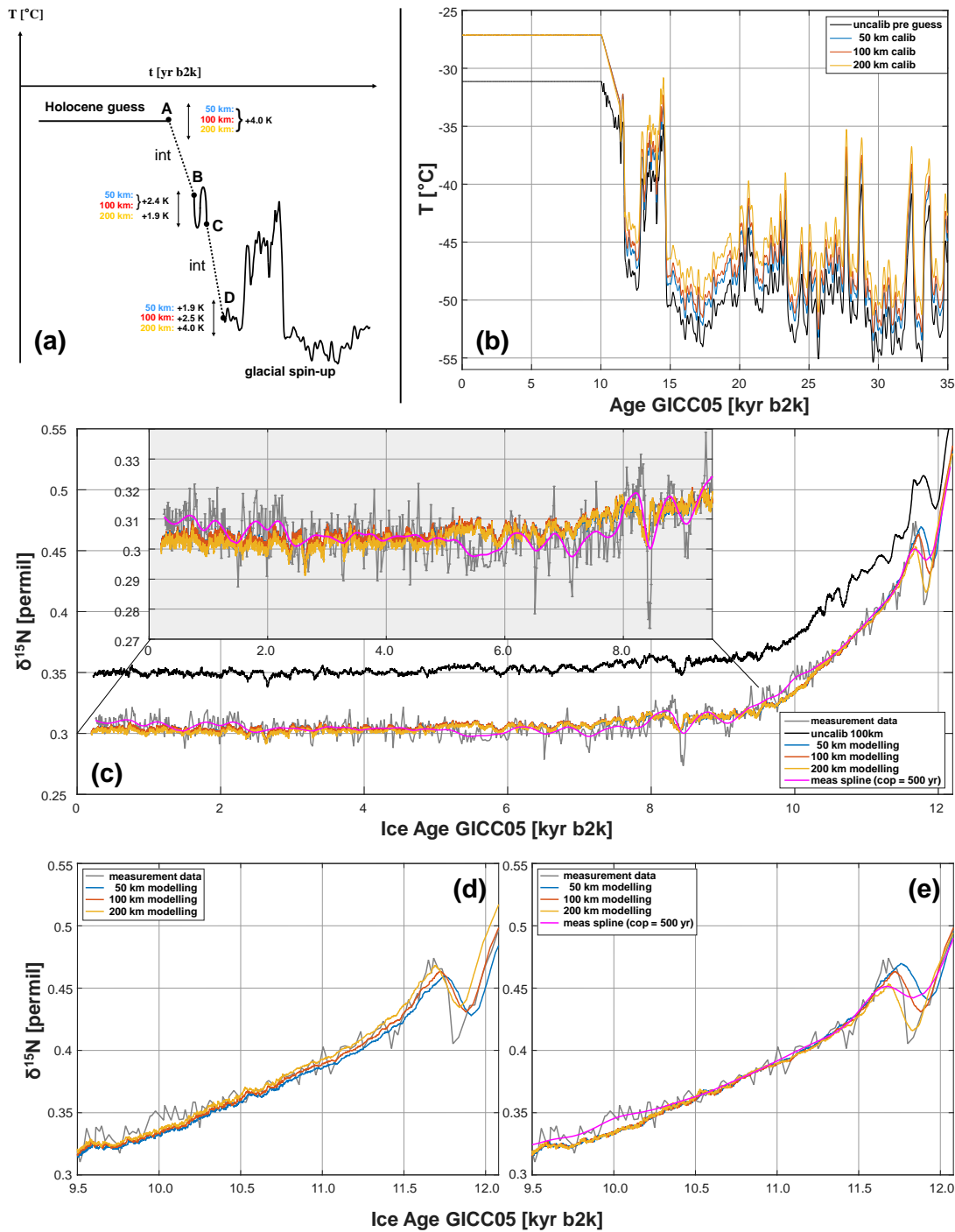
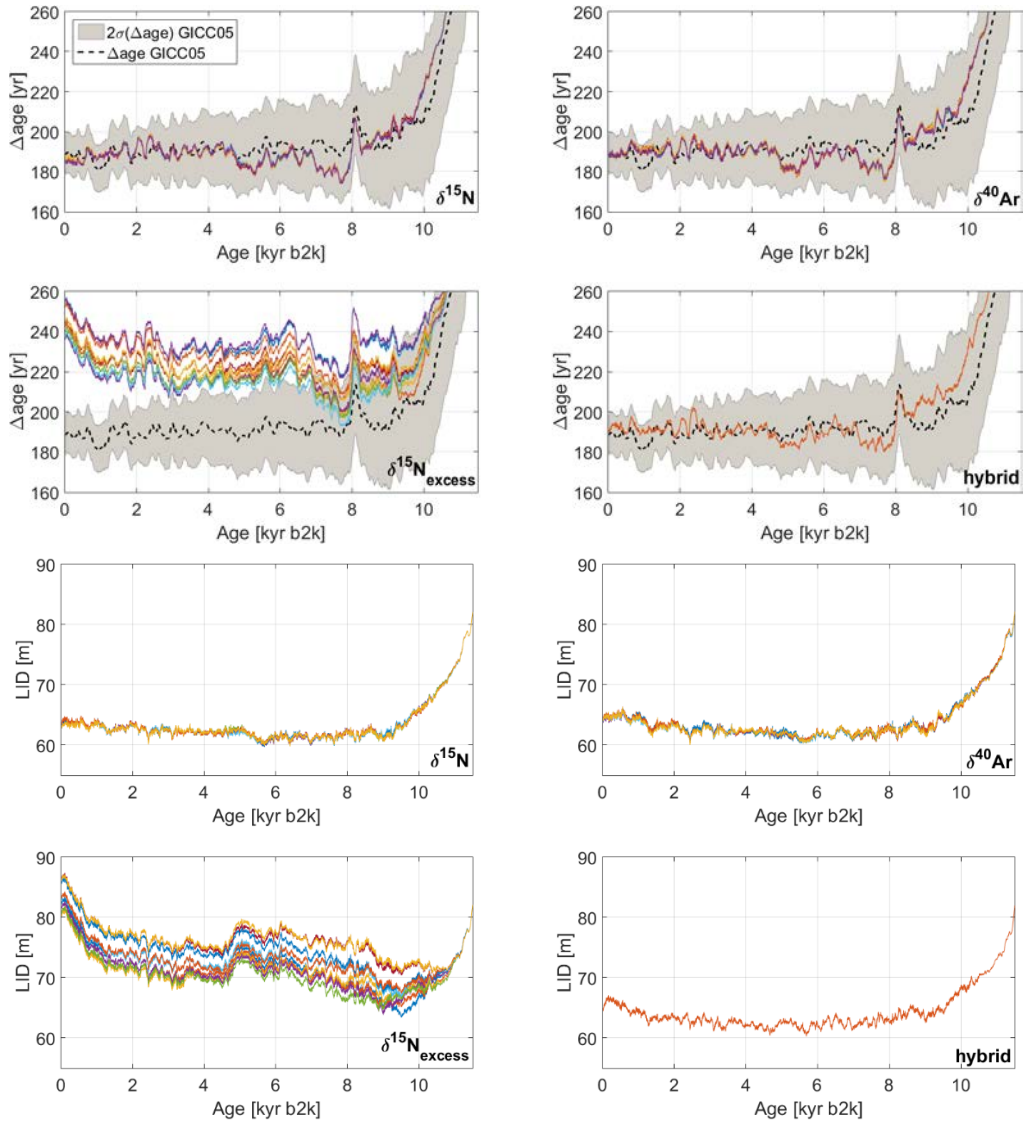


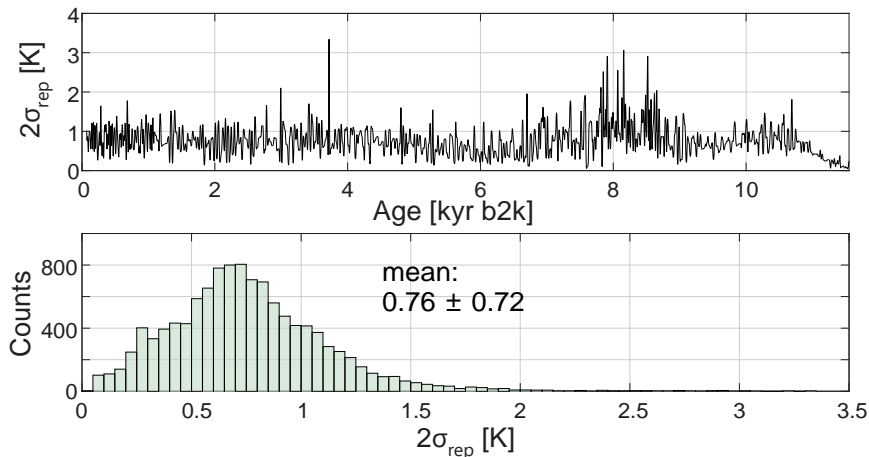
Figure S2: (a): Adjustment scheme of the prior inputs for different accumulation-rate scenarios (see text), the time of A-D are as follows: A = 10050 yr b2k, B = 11350 yr b2k, C = 11630 yr b2k, D = 11750 yr b2k; “int” refers to the regions of linear interpolation between the respective times after adjustment; the temperature offsets for the three parts of the time-series were found using Nelder-Mead Simplex minimisation (Lagarias et al., 1998). (b): Initial spin-up temperature (black line) with glacial section from Buizert et al. (2014) and Cuffey and Clow (1997), and adjusted input temperatures for different accumulation-rate scenarios (50 km: blue, 100 km: red, 200 km: yellow). (c): Raw (grey) and splined (purple) $\delta^{15}\text{N}$ measurement data (Kobashi et al., 2008), and modelled $\delta^{15}\text{N}$ time-series using the initial spin-up (black), or the adjusted spin-up temperature inputs together with the respective accumulation-rates (50 km: blue, 100 km: red, 200 km: yellow). (d): Minimization window for the calibration: modelled $\delta^{15}\text{N}$ time-series using the 100 km calibration for all accumulation-rate scenarios showing that only the red curve (100 km) matches the introductory flank (11.8 kyr to 12.2 kyr) in the middle of variance of the measurement data sufficiently whereas the blue (50 km) and yellow (200 km) curve show divergences lasting for about 2 kyr (10 kyr to 12 kyr b2k). (e): Minimization window for the adjustment: modelled $\delta^{15}\text{N}$ time-series using the adjusted spin-up temperature input scenarios showing good agreement between the respective $\delta^{15}\text{N}$ scenarios.

S3: Modelling results for the different gas-isotope targets



5 **Figure S3: Upper four plots: Modelled gasage-iceage-differences (Δ age) for all isotope species (top left: $\delta^{15}\text{N}$; top right: $\delta^{40}\text{Ar}$; bottom left: $\delta^{15}\text{N}_{\text{excess}}$; bottom right: hybrid) and the hybrid solution compared to the Δ age for GISP2 from GICC05 (dashed black line). Notice the large spread for $\delta^{15}\text{N}_{\text{excess}}$ -fitting of about 20 yr to 30 yr.**

Bottom four plots: Modelled lock-in-depth (LID) as a measure for the firn column height for all isotope species (top left: $\delta^{15}\text{N}$; top right: $\delta^{40}\text{Ar}$; bottom left: $\delta^{15}\text{N}_{\text{excess}}$; bottom right: hybrid) and the hybrid solution. Notice the large spread for $\delta^{15}\text{N}_{\text{excess}}$ -fitting of about 10 m.



10

Figure S4: Reproducibility of temperature solutions between 10 runs using Goujon model and $\delta^{15}\text{N}_{\text{excess}}$ target. (Reproducibility is more than 2.7 times better as for the Schwander model)

| target | quantity | 50 km | 100 km | 200 km | information |
|--|--|-----------------|-----------------|-------------------|-------------|
| $\delta^{15}\text{N}$ | mean($2\sigma_{\text{miss}}$) | 4.36 ± 0.40 | 3.71 ± 0.38 | 4.09 ± 0.19 | fit |
| | (best fit) | (3.64) | (3.27) | (3.82) | |
| | [permeg] | | | | |
| | $2\sigma_{\text{mismatch}}$ | 3.83 | 3.19 | 3.65 | fit |
| | mean solution | | | | |
| | [permeg] | | | | |
| | mean($2\sigma_{\text{rep}}$) | 2.09 ± 1.64 | 2.16 ± 1.39 | 1.68 ± 1.14 | rep |
| | [permeg] | | | | |
| T($\delta^{15}\text{N}$) | mean($2\sigma_{\text{rep}}$) | 0.21 ± 0.17 | 0.22 ± 0.13 | 0.17 ± 0.12 | rep |
| | [K] | | | | |
| $\delta^{40}\text{Ar}/4$ | mean($2\sigma_{\text{miss}}$) | | | 3.80 ± 0.24 | fit |
| | (best fit) | | | (3.44) | |
| | [permeg] | | | | |
| | $2\sigma_{\text{miss}}$ | | | | fit |
| | mean solution | | | 2.79 | |
| | [permeg] | | | | |
| | mean($2\sigma_{\text{rep}}$) | | | 2.58 ± 1.77 | rep |
| | [permeg] | | | | |
| T($\delta^{40}\text{Ar}$) | mean($2\sigma_{\text{rep}}$) | | | 0.26 ± 0.18 | rep |
| | [K] | | | | |
| $\delta^{15}\text{N}_{\text{excess}}$ | mean($2\sigma_{\text{miss}}$) | | | 2.93 ± 0.49 | fit |
| | (best fit) | | | (2.13) | |
| | [permeg] | | | | |
| | $2\sigma_{\text{miss}}$ | | | | fit |
| | mean solution | | | 5.43* | |
| | [permeg] | | | | |
| | mean($2\sigma_{\text{rep}}$) | | | 1.28 ± 2.14 | rep |
| | [permeg] | | | | |
| T($\delta^{15}\text{N}_{\text{excess}}$) | mean($2\sigma_{\text{rep}}$) [K] | | | $2.04 \pm 1.90^*$ | rep |
| Hybrid | $2\sigma_{\text{mismatch}}(\delta^{15}\text{N})$ | | | 28.50 | fit |
| ($\delta^{15}\text{N}$ lf, | $2\sigma_{\text{mismatch}}(\delta^{40}\text{Ar})$ | | | 27.73 | |
| $\delta^{15}\text{N}_{\text{excess}}$ hf) | $2\sigma_{\text{mismatch}}(\delta^{15}\text{N}_{\text{excess}})$ | | | 7.57 | |
| | [permeg] | | | | |

Table S2: Goodness of the fits (fit) and reproducibility (rep) using the firn-model from Schwander et al. (1997): For all gas-isotope targets 10 runs were conducted for the 200 km accumulation-rate scenario. Additionally, 10 runs were conducted for each accumulation-rate scenario for $\delta^{15}\text{N}$ as target. mean($2\sigma_{\text{mismatch}}$) is the mean of the doubled standard deviation of the differences between modelled and measured data for all runs plus minus the 2σ deviation between the runs. mean($2\sigma_{\text{mismatch}}$) is a measure for the mean misfit between the modelled and the target data. mean($2\sigma_{\text{solution}}$) is the mean of the doubled standard deviations per age point over the 10 runs and a measure for the spread of the temperature solutions.

5

S4: Boundary effect

While running the gas-isotope fitting algorithm several times on the same target, we notice a boundary effect for the last 500 yr to 1 kyr to today when using the Schwander et al. as well as the Goujon et al. firn-model. Here different temperature solutions emerge while the rest of time-series is highly reproducible (fig. S5c,d and sect. 3.1.1). Figure S5 shows that issue for $\delta^{15}\text{N}$ -fitting using the Goujon et al. firn-model. Fitting of $\delta^{15}\text{N}$ leads to solutions with increasing (fig. S5a: red lines), decreasing (fig. S5a: blue lines) or even flat (fig. S5a: green lines) millennial temperature trends in this time-window, but fitting the isotopes to the same precision (fig. S5b,c). The reason for that is a cancellation between opposite trends of the thermal diffusion (fig. S5e) and the gravitational fractionation components (fig. S5f) of the modelled $\delta^{15}\text{N}$ signals for those low magnitude signals (about 20 permeg). For example, a long-term cooling trend will increase the diffusive firn column (and so the LID) due to decelerated densification of the firn, leading to an increase of the gravitational component of $\delta^{15}\text{N}$ (fig. S5f,h: blue lines). On the same time the cooling leads to a decrease of the temperature gradient (ΔT_{firn}) over the firn column (fig. S5g) which follows in first order the surface temperature trend. The decrease in ΔT_{firn} leads to a decrease of the thermal diffusion component (fig. S5e). The same happens for the warming temperature trends but with opposite direction for LID(t) and ΔT_{firn} (t). Only in the last 500 yr and due to the lack of data availability we experienced this boundary effect. This effect can be understood by the influence of data on the past values. The fitting algorithm works from past into future direction. If a “wrong” temperature trend would be created, leading to the same $\delta^{15}\text{N}$ signal as for the “right” temperature trend, there will be a certain point in time in future direction where the modelled isotope signals will drift away from the measured isotope targets leaving the range of the cancellation. Unfortunately, at the boundary of the gas-isotope record, there is no further data available to stabilize the temperature solutions. Using this explanation for testing the reproducibility (sect. 3.1.1), we extended the measurement data for 1 kyr into the future by adding constant isotope values calculated from the mean of the isotope data over the recent 1 kyr. This extension leads to stable temperature solution even for the last 1 kyr and forces the algorithm to produce the flat temperature solution in this time-window. Unfortunately, it cannot be determined in that way which temperature trend for the last 1 kyr is the most realistic case by fitting the isotope data as single targets. To overcome this problem, an additional constraint is needed. For that issue we use an analogue to Kobashi et al. (2017) (see supplement fig. S4 there), namely using the measured borehole temperature profile for the GISP2 site (Alley and Koci, 1990; Clow et al., 1996). The firn-model from Goujon et al. (2003) provides the possibility to model the temperature profile through the ice-sheet. As the measurement target data ($\delta^{15}\text{N}$) starts from 255 yr b2k (GICC05 ice ages) which refers to 70 yr b2k (gas ages, modelled from $T(\delta^{15}\text{N})$) we had to extend the temperature from 70 yr b2k to 7 yr b2k, the time when the temperature profile was measured. For this extension we use Greenland Summit temperatures from Kobashi et al. (2017), estimated from correlating coastal and Summit instrumental air temperatures. Figure S5i shows the modelled temperature profile for all 10 temperature scenarios at the boundary of the gas-isotope record. To correctly model the measured temperature profile, we had to shift each of the 10 temperature estimates by a constant offset of -1 K for the entire Holocene (70 yr b2k to 11.65 kyr b2k), changing the absolute temperature but not the anomalies. The reason for this necessity remains unknown yet. It is clearly visible that only those scenarios with a cooling trend (blue lines) lead to an acceptable shape when compared to the measured borehole profile. Additionally, it is possible to use $\delta^{40}\text{Ar}$ data as second constraint (fig. S5j). Comparing the measured and modelled $\delta^{40}\text{Ar}$ data also favours the temperature estimates showing the cooling trend, because these solutions are leading to modelled $\delta^{40}\text{Ar}$ with the smallest mismatch to the measured data.

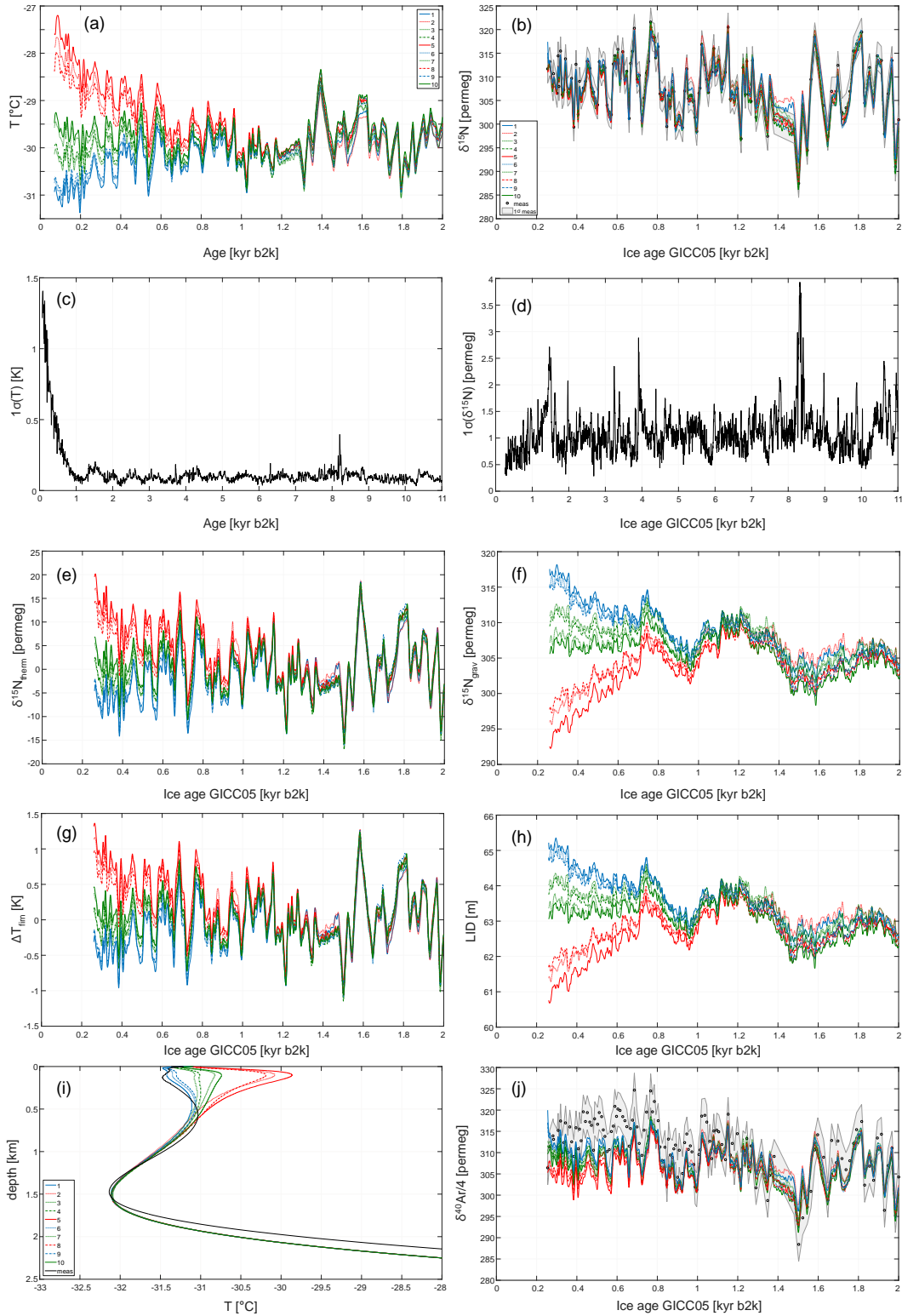


Figure S5: (a): Deviation of reconstructed temperatures on the boundary of the gas-isotope record between 10 runs of the fitting algorithm. (b): Measured $\delta^{15}\text{N}$ record (dots) with minimal 1σ uncertainty (grey area) and $\delta^{15}\text{N}$ -fits modelled using the temperatures from (a). (c) Standard deviation (spread) between the 10 temperatures from (a) showing a decreasing reproducibility on the boundary for the last 0.5-1.0 kyr to today. (d): Standard deviation (spread) between the 10 $\delta^{15}\text{N}$ -fits does not show decreasing reproducibility on the boundary for the last 500 yr to 1 kyr to today. (e): Thermal fractionation component of $\delta^{15}\text{N}$ modelled using the reconstructed temperatures of (a). (f) Component of $\delta^{15}\text{N}$ due to gravitational settling modelled using the reconstructed temperatures of (a). (g) Firn temperature gradient modelled using the reconstructed temperatures of (a). (h) Lock-in-depth modelled using the reconstructed temperatures of (a). (i) Temperature profile through the ice-sheet modelled using the reconstructed temperatures of (a). (j): Measured $\delta^{40}\text{Ar}/4$ record (dots) with minimal 1σ uncertainty (grey area) and $\delta^{40}\text{Ar}/4$ modelled using the temperatures from (a).

S5: Temperature estimates when fitting different gas isotope targets

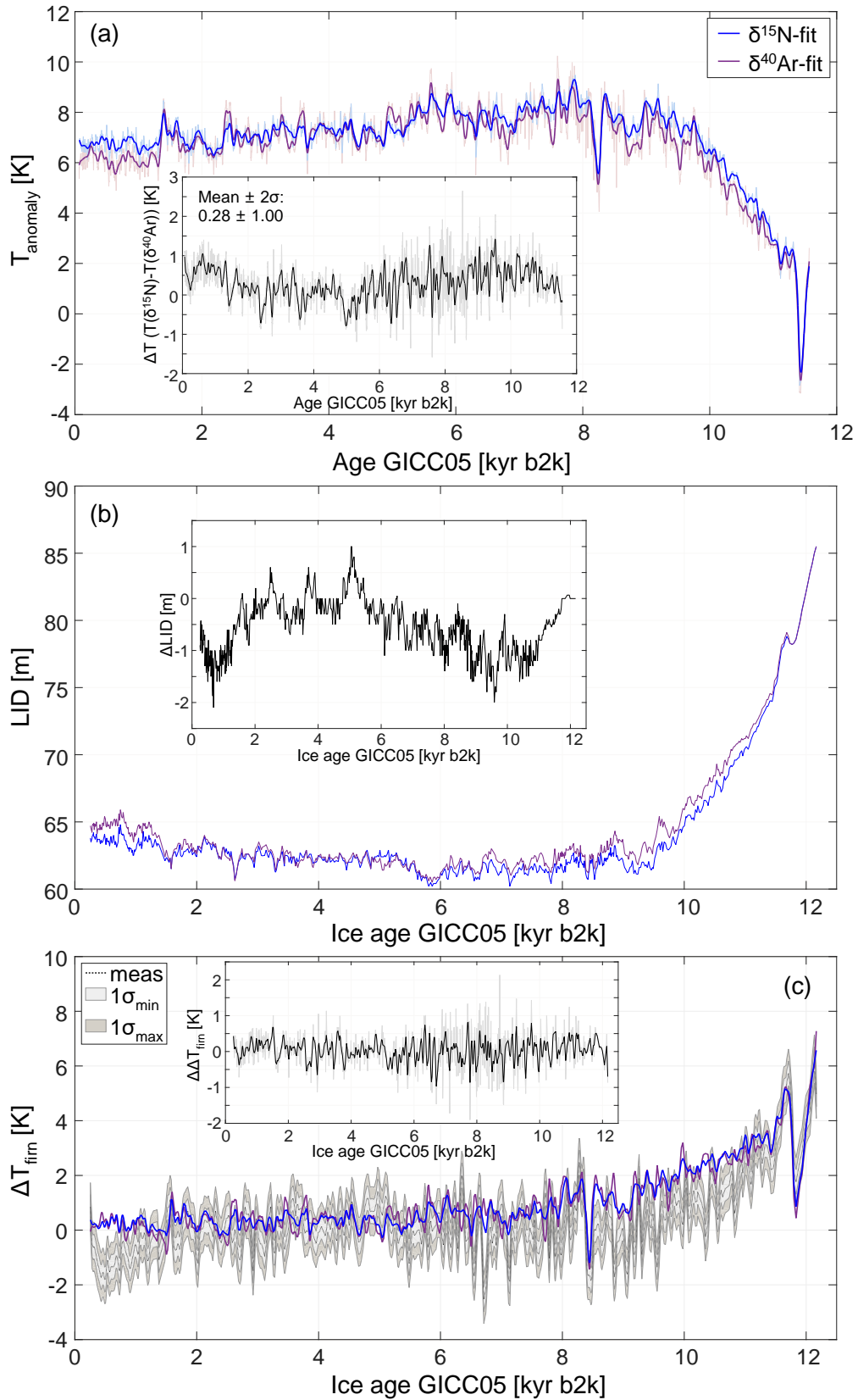


Figure S6: Comparison between temperature anomalies (a), LID (b) and ΔT_{firn} (c) reconstructed from $\delta^{15}\text{N}$ (blue) and $\delta^{40}\text{Ar}$ (purple) using the model from Schwander et al. (1997). Black curves in the subplots show the differences between the $\delta^{15}\text{N}$ - and $\delta^{40}\text{Ar}$ -fits for the given quantities. In subplot (c) the modelled data is shown together with measured data (meas, dotted line) from Kobashi et al. (2008) with minimal and maximal 1σ uncertainty calculated from uncertainties given in tab. 1 with eq. (4).

5

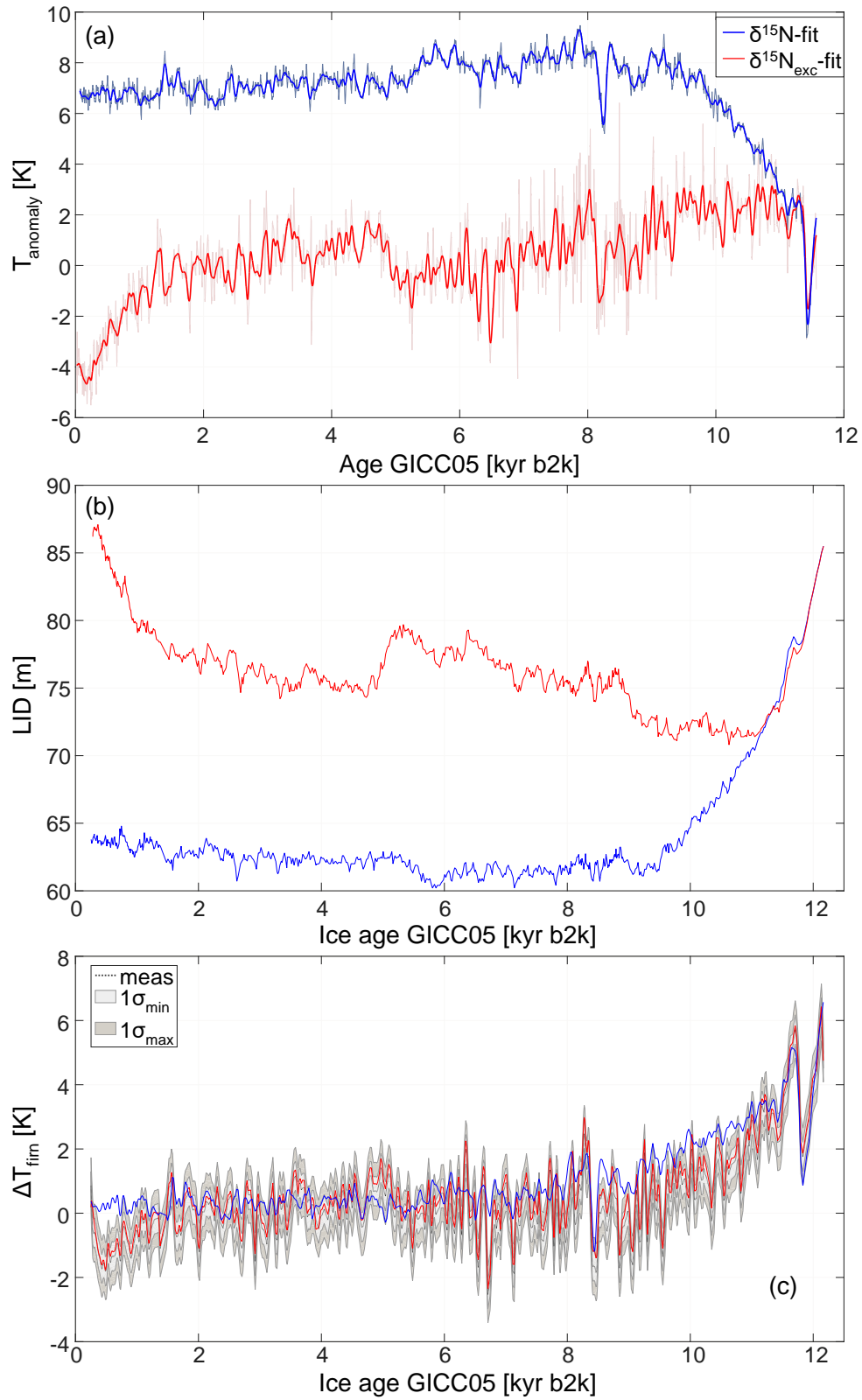


Figure S7: Comparison between temperature anomalies (a), LID (b) and ΔT_{firn} (c) reconstructed from $\delta^{15}\text{N}$ (blue) and $\delta^{15}\text{N}_{\text{excess}}$ (red) using the model from Schwander et al. (1997). In subplot (c) the modelled data is shown together with measured data (meas, dotted line) from Kobashi et al. (2008b) with minimal and maximal 1σ uncertainty calculated from uncertainties given in tab.1 with eq. (4).

5

S6: Correlation analysis of the temperature estimates when fitting different gas isotope targets

A comparison of the reconstructions is conducted by calculating the Pearson's correlation coefficients between the estimates after low-pass filtering (cop = 50 yr, tab. S3) and band-pass filtering in three periodic-time bands: multi-millennial (1000 yr-4000 yr, tab.S4), multi-centennial (band: 200 yr-1000 yr, tab.S5), and multi-decadal (band: 50 yr-200 yr, tab.S6). As the slightly different Δ age regimes can alter the correlation for the multi-decadal band, we conducted sample-cross-correlation (*xcf*, Box et al., 1994) to find the time-lag between the estimates with maximum correlation. The correlations were calculated in the time-window 0.5-11.5 kyr b2k to account for the boundary effect (sect. S4). Statistical significance (p-value) was calculated using the approach of Ebisuzaki (1997).

| | T($\delta^{15}\text{N}$) S-Model | T($\delta^{40}\text{Ar}$) S-Model | T(hyb) S-Model | T($\delta^{15}\text{N}_{\text{excess}}$) S-Model-bf | T($\delta^{15}\text{N}_{\text{excess}}$) S-Model-m | T($\delta^{15}\text{N}$) G-Model | T($\delta^{40}\text{Ar}$) G-Model | T(hyb) G-Model | T($\delta^{15}\text{N}_{\text{excess}}$) G-Model |
|--|---------------------------------------|--|-------------------|--|---|---------------------------------------|--|-------------------|---|
| T($\delta^{15}\text{N}$) S-Model | | 0.96 | 0.83 | -0.16 (0.25) | 0.13 (0.31) | 0.99 | 0.95 | 0.79 | 0.31 (0.13) |
| T($\delta^{40}\text{Ar}$) S-Model | 0.96 | | 0.74 | -0.19 (0.22) | 0.05 (0.42) | 0.95 | 0.98 | 0.70 | 0.26 (0.21) |
| T(hybrid) S-Model | 0.83 | 0.74 | | -0.16 (0.23) | 0.12 (0.34) | 0.81 | 0.71 | 0.98 | 0.57 |
| T($\delta^{15}\text{N}_{\text{excess}}$) S-Model-bf | -0.16 (0.25) | -0.19 (0.22) | -0.16 (0.23) | | 0.88 | -0.12 (0.29) | -0.16 (0.25) | -0.21 (0.16) | 0.19 (0.18) |
| T($\delta^{15}\text{N}_{\text{excess}}$) S-Model-m | 0.13 (0.31) | 0.05 (0.42) | 0.12 (0.34) | 0.88 | | 0.16 (0.26) | 0.08 (0.39) | 0.06 (0.41) | 0.30 (0.08) |
| T($\delta^{15}\text{N}$) G-Model | 0.99 | 0.95 | 0.81 | -0.12 (0.29) | 0.16 (0.26) | | 0.95 | 0.78 | 0.36 (0.05) |
| T($\delta^{40}\text{Ar}$) G-Model | 0.95 | 0.98 | 0.71 | -0.16 (0.25) | 0.08 (0.39) | 0.95 | | 0.67 | 0.27 (0.17) |
| T(hybrid) G-Model | 0.79 | 0.70 | 0.98 | -0.21 (0.16) | 0.06 (0.41) | 0.78 | 0.67 | | 0.53 |
| T($\delta^{15}\text{N}_{\text{excess}}$) G-Model | 0.31 (0.13) | 0.26 (0.21) | 0.57 | 0.19 (0.18) | 0.30 (0.08) | 0.36 (0.05) | 0.27 (0.17) | 0.53 | |

Table S3: correlation coefficient r, statistical significance (p): low-pass cop = 50 yr, if not otherwise stated, p < 0.01.

| | T($\delta^{15}\text{N}$) S-Model | T($\delta^{40}\text{Ar}$) S-Model | T(hybrid) S-Model | T($\delta^{15}\text{N}_{\text{excess}}$) S-Model-bf | T($\delta^{15}\text{N}_{\text{excess}}$) S-Model-m | T($\delta^{15}\text{N}$) G-Model | T($\delta^{40}\text{Ar}$) G-Model | T(hybrid) G-Model | T($\delta^{15}\text{N}_{\text{excess}}$) G-Model |
|--|---------------------------------------|--|----------------------|--|---|---------------------------------------|--|----------------------|---|
| T($\delta^{15}\text{N}$) S-Model | | 0.94 | 0.75 | 0.61 | 0.68 | 0.97 | 0.85 | 0.64 | 0.66 |
| T($\delta^{40}\text{Ar}$) S-Model | 0.94 | | 0.70 | 0.48 | 0.54 | 0.91 | 0.90 | 0.64 | 0.54 |
| T(hybrid) S-Model | 0.75 | 0.70 | | 0.86 | 0.89 | 0.74 | 0.60 | 0.97 | 0.89 |
| T($\delta^{15}\text{N}_{\text{excess}}$) S-Model-bf | 0.61 | 0.48 | 0.86 | | 0.96 | 0.67 | 0.46 | 0.78 | 0.98 |
| T($\delta^{15}\text{N}_{\text{excess}}$) S-Model-m | 0.68 | 0.54 | 0.89 | 0.96 | | 0.70 | 0.51 | 0.81 | 0.98 |
| T($\delta^{15}\text{N}$) G-Model | 0.97 | 0.91 | 0.74 | 0.66 | 0.70 | | 0.88 | 0.64 | 0.69 |
| T($\delta^{40}\text{Ar}$) G-Model | 0.85 | 0.90 | 0.60 | 0.46 | 0.51 | 0.88 | | 0.52 | 0.51 |
| T(hybrid) G-Model | 0.64 | 0.64 | 0.97 | 0.78 | 0.81 | 0.64 | 0.52 | | 0.82 |
| T($\delta^{15}\text{N}_{\text{excess}}$) G-Model | 0.66 | 0.54 | 0.89 | 0.98 | 0.98 | 0.69 | 0.51 | 0.82 | |

Table S4: correlation coefficient r, statistical significance (p): band-pass: 1000-4000yr (multi-millennial, detrended), if not otherwise stated, p < 0.01.

| | T($\delta^{15}\text{N}$) S-Model | T($\delta^{40}\text{Ar}$) S-Model | T(hybrid) S-Model | T($\delta^{15}\text{N}_{\text{excess}}$) S-Model-bf | T($\delta^{15}\text{N}_{\text{excess}}$) S-Model-m | T($\delta^{15}\text{N}$) G-Model | T($\delta^{40}\text{Ar}$) G-Model | T(hyb) G-Model | T($\delta^{15}\text{N}_{\text{excess}}$) G-Model |
|--|---------------------------------------|--|----------------------|--|---|---------------------------------------|--|-------------------|---|
| T($\delta^{15}\text{N}$) S-Model | | 0.87 | 0.59 | 0.54 | 0.56 | 0.96 | 0.87 | 0.51 | 0.59 |
| T($\delta^{40}\text{Ar}$) S-Model | 0.87 | | 0.18 (0.05) | 0.20 (0.03) | 0.19 (0.05) | 0.82 | 0.94 | 0.17 (0.07) | 0.19 (0.05) |
| T(hybrid) S-Model | 0.59 | 0.18 (0.05) | | 0.73 | 0.85 | 0.63 | 0.24 (0.02) | 0.95 | 0.96 |
| T($\delta^{15}\text{N}_{\text{excess}}$) S-Model-bf | 0.54 | 0.20 (0.03) | 0.73 | | 0.97 | 0.58 | 0.27 | 0.54 | 0.87 |
| T($\delta^{15}\text{N}_{\text{excess}}$) S-Model-m | 0.56 | 0.19 (0.05) | 0.85 | 0.97 | | 0.60 | 0.26 (0.01) | 0.70 | 0.95 |
| T($\delta^{15}\text{N}$) G-Model | 0.96 | 0.82 | 0.63 | 0.58 | 0.60 | | 0.88 | 0.57 | 0.63 |
| T($\delta^{40}\text{Ar}$) G-Model | 0.87 | 0.94 | 0.24 (0.02) | 0.27 | 0.26 (0.01) | 0.88 | | 0.23 (0.02) | 0.25 (0.01) |
| T(hybrid) G-Model | 0.51 | 0.17 (0.07) | 0.95 | 0.54 | 0.70 | 0.57 | 0.23 (0.02) | | 0.84 |
| T($\delta^{15}\text{N}_{\text{excess}}$) G-Model | 0.59 | 0.19 (0.05) | 0.96 | 0.87 | 0.95 | 0.63 | 0.25 (0.01) | 0.84 | |

Table S5: correlation coefficient r , statistical significance (p): band-pass: 200-1000yr (multi-centennial), if not otherwise stated, $p < 0.01$.

| x/y | T($\delta^{15}\text{N}$) S-Model | T($\delta^{40}\text{Ar}$) S-Model | T(hybrid) S-Model | T($\delta^{15}\text{N}_{\text{excess}}$) S-Model-bf | T($\delta^{15}\text{N}_{\text{excess}}$) S-Model-m | T($\delta^{15}\text{N}$) G-Model | T($\delta^{40}\text{Ar}$) G-Model | T(hybrid) G-Model | T($\delta^{15}\text{N}_{\text{excess}}$) G-Model |
|--|---|--|--|--|---|--|---|---|---|
| T($\delta^{15}\text{N}$) S-Model | | 0.67 [†] <i>0.69</i> [-4] | 0.33 [†] | 0.06 (0.17) [†] <i>0.13</i> [-39] | 0.13 (0.01) [†] <i>0.18</i> [-19] | 0.95 [†] <i>0.97</i> [-3] | 0.67 [†] <i>0.69</i> [-4] | 0.33 [†] | 0.29 [†] <i>0.31</i> [-6] |
| T($\delta^{40}\text{Ar}$) S-Model | 0.67 [†] <i>0.69</i> [-4] | | -0.43 [†] <i>-0.44</i> [-3] | 0.25 [†] <i>-0.41</i> [-42] | 0.10 (0.07) [†] <i>-0.36</i> [-29] | 0.69 [†] | 0.99 [†] | -0.43 [†] | 0.12 (0.02) [†] <i>-0.38</i> [-18] |
| T(hybrid) S-Model | 0.33 [†] | -0.43 [†] <i>-0.44</i> [-3] | | -0.23 [†] <i>0.71</i> [-39] | -0.12 (0.05) [†] <i>0.69</i> [-25] | 0.31 [†] | -0.43 [†] <i>-0.45</i> [2] | 0.96 [†] <i>0.98</i> [3] | 0.63 [†] <i>0.84</i> [-11] |
| T($\delta^{15}\text{N}_{\text{excess}}$) S-Model-bf | 0.06 (0.17) [†] <i>0.13</i> [-39] | 0.25 [†] <i>-0.41</i> [-42] | -0.23 [†] <i>0.71</i> [-39] | | 0.69 [†] <i>0.95</i> [11] | 0.08 (0.10) [†] <i>0.12</i> [36] | 0.27 [†] <i>-0.41</i> [42] | -0.34 [†] <i>0.74</i> [43] | 0.06 [†] <i>0.79</i> [24] |
| T($\delta^{15}\text{N}_{\text{excess}}$) S-Model-m | 0.13 (0.01) [†] <i>0.18</i> [-19] | 0.10 (0.07) [†] <i>-0.36</i> [-29] | -0.12 (0.05) [†] <i>0.69</i> [-25] | 0.69 [†] <i>0.95</i> [11] | | 0.15 [†] <i>0.18</i> [13] | 0.11 (0.05) [†] <i>-0.37</i> [29] | -0.05 (0.25) [†] <i>0.72</i> [29] | 0.59 [†] <i>0.81</i> [12] |
| T($\delta^{15}\text{N}$) G-Model | 0.95 [†] <i>0.97</i> [-3] | 0.69 [†] | 0.31 [†] | 0.08 (0.10) [†] <i>0.12</i> [36] | 0.15 [†] <i>0.18</i> [13] | | 0.70 [†] | 0.30 [†] | 0.31 [†] |
| T($\delta^{40}\text{Ar}$) G-Model | 0.67 [†] <i>0.69</i> [-4] | 0.99 [†] | -0.43 [†] <i>-0.45</i> [2] | 0.27 [†] <i>-0.41</i> [42] | 0.11 (0.05) [†] <i>-0.37</i> [29] | 0.70 [†] | | -0.45 [†] | -0.12 (0.03) [†] <i>-0.40</i> [-18] |
| T(hybrid) G-Model | 0.33 [†] | -0.43 [†] | 0.96 [†] <i>0.98</i> [3] | -0.34 [†] <i>0.74</i> [43] | -0.05 (0.25) [†] <i>0.72</i> [29] | 0.30 [†] | -0.45 [†] | | -0.47 [†] <i>0.83</i> [-15] |
| T($\delta^{15}\text{N}_{\text{excess}}$) G-Model | 0.29 [†] <i>0.31</i> [-6] | 0.12 (0.02) [†] <i>-0.38</i> [-18] | 0.63 [†] <i>0.84</i> [-11] | 0.06 [†] <i>0.79</i> [24] | 0.59 [†] <i>0.81</i> [12] | 0.31 [†] | -0.12 (0.03) [†] <i>-0.40</i> [-18] | -0.47 [†] <i>0.83</i> [-15] | |

Table S6: correlation coefficient r , statistical significance (p) [†] maximum correlation coefficient for cross-correlation $\text{xcf}(x/y)$ on respective [lag], unit of [lag] is yr. band-pass: 50-200yr (multi-decadal), if not otherwise stated, $p < 0.01$.

S7: Correlations of the temperature estimates for the different gas isotope targets versus Kobashi et al. 2017 (T_K) and Buizert et al. 2018 (T_B)

| | Kobashi et al. 2017 (T_K)* | | | | Buizert et al. 2018 (T_B)** | | | |
|--|--------------------------------|--|---|--|---------------------------------|--|---|--|
| | low-pass cop [yr] 50 | band-pass [yr] 50-200 (multi- decadal) | band-pass [yr] 200-1000 (multi- centennial) | band- pass [yr] 1000-4000 (multi- millennial) | low-pass cop [yr] 50 | band-pass [yr] 50-200 (multi- decadal) | band-pass [yr] 200-1000 (multi- centennial) | band-pass [yr] 1000-4000 (multi- millennial) |
| T($\delta^{15}N$) S-Model | 0.81 | 0.21 _‡ 0.26 [12] | 0.61 | 0.50 | 0.95 | 0.22 _‡ 0.30 [17] | 0.61 | 0.67 |
| T($\delta^{40}Ar$) S-Model | 0.72 | -0.25 _‡ -0.37 [12] | 0.25 (0.01) | 0.46 | 0.92 | 0.24 _‡ 0.26 [10] | 0.54 | 0.63 |
| T(hybrid) S-Model | 0.87 | 0.67 _‡ 0.81 [9] | 0.90 | 0.78 | 0.79 | -0.01 (0.44) _‡ | 0.39 | 0.50 (0.01) |
| T($\delta^{15}N_{excess}$) S-Model-bf | 0.02 (0.47) | -0.06 (0.20) _‡ 0.67 [-30] | 0.79 | 0.78 | -0.22 (0.31) | -0.05 (0.25) _‡ | 0.38 | 0.35 (0.07) |
| T($\delta^{15}N_{excess}$) S-Model-m | 0.30 (0.08) | 0.42 _‡ 0.68 [-16] | 0.87 | 0.76 | 0.15 (0.38) | 0.06 (0.19) _‡ | 0.38 | 0.48 |
| T($\delta^{15}N$) G-Model | 0.82 | 0.24 _‡ 0.27 [9] | 0.66 | 0.51 | 0.93 | 0.26 _‡ 0.29 [11] | 0.63 | 0.57 |
| T($\delta^{40}Ar$) G-Model | 0.70 | -0.25 _‡ -0.37 [12] | 0.30 | 0.36 (0.06) | 0.90 | 0.24 _‡ 0.26 [10] | 0.61 | 0.45 (0.04) |
| T(hybrid) G-Model | 0.83 | 0.55 _‡ 0.82 [13] | 0.80 | 0.79 | 0.75 | -0.02 (0.42) _‡ | 0.35 | 0.42 (0.06) |
| T($\delta^{15}N_{excess}$) G-Model | 0.59 | 0.73 _‡ 0.74 [-3] | 0.92 | 0.78 | 0.31 (0.02) | 0.06 (0.18) _‡ | 0.40 | 0.45 (0.02) |
| T_K | | | | | 0.82** | 0.05** (0.25) _‡ | 0.48** | 0.52** (0.03) |
| T_B | 0.82** | 0.05** (0.25) _‡ | 0.48** | 0.52** (0.03) | | | | |

Table S7: Correlation coefficient r , statistical significance (p) ‡ maximum correlation coefficient for cross-correlation $xcf(x/y)$ on respective [lag], if not otherwise stated: $p < 0.01$. *The correlations between the Kobashi et al. (2017) and our data were calculated in the time-window 0.5-11.5 kyr b2k. **The correlations between the Buizert et al. (2018) and our data as well as between the Kobashi et al. (2017) and the Buizert et al. (2018) data were calculated in time-window 4.0-11.5 kyr b2k.

5

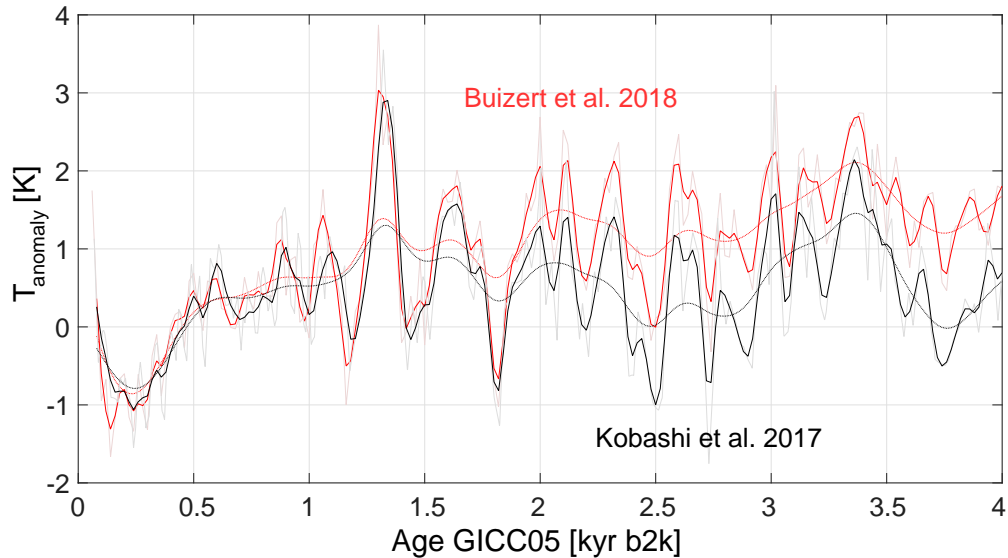


Figure S8: Comparison of the reconstructed temperatures anomalies (rel. to last 1 kyr) of Buizert et al. (2018) (red lines) and Kobashi et al. (2017) (black lines) for the last 4 kyr. Thick lines show data smooth with 100 yr cut-off, dotted line with 500 yr cut-off, thin lines are 20 yr resolution.

5 References:

- Alley, R. B. and Koci, B. R.: Recent warming in central Greenland?, *Ann. Glaciol.*, 14, 6–8, doi:10.3189/S0260305500008144, 1990.
- Box, G. E. P., Jenkins, G. M. and Reinsel, G. C.: *Time Series Analysis - Forecasting and Control.*, 1994.
- Buizert, C., Gkinis, V., Severinghaus, J. P., He, F., Lecavalier, B. S., Kindler, P., Leuenberger, M., Carlson, A. E.,
 10 Vinther, B., Masson-Delmotte, V., White, J. W. C., Liu, Z., Otto-Bliesner, B. and Brook, E. J.: Greenland temperature response to climate forcing during the last deglaciation., *Science*, 345(6201), 1177–80, doi:10.1126/science.1254961, 2014.
- Buizert, C., Keisling, B. A., Box, J. E., He, F., Carlson, A. E., Sinclair, G. and DeConto, R. M.: Greenland-Wide Seasonal Temperatures During the Last Deglaciation, *Geophys. Res. Lett.*, 45(4), 1905–1914,
 15 doi:10.1002/2017GL075601, 2018.
- Clow, G. D., Saltus, R. W. and Waddington, E. D.: A new high-precision borehole-temperature logging system used at GISP2, Greenland, and Taylor Dome, Antarctica, *J. Glaciol.*, 42(142), 576–584, doi:10.1017/S0022143000003555, 1996.
- Cuffey, K. M. and Clow, G. D.: Temperature, accumulation, and ice sheet elevation in central Greenland through
 20 the last deglacial transition, *J. Geophys. Res. Ocean.*, 102(C12), 26383–26396, doi:10.1029/96JC03981, 1997.
- Ebisuzaki, W.: A method to estimate the statistical significance of a correlation when the data are serially correlated, *J. Clim.*, 10(9), 2147–2153, doi:10.1175/1520-0442(1997)010<2147:AMTETS>2.0.CO;2, 1997.
- Goujon, C., Barnola, J.-M. and Ritz, C.: Modeling the densification of polar firn including heat diffusion: Application to close-off characteristics and gas isotopic fractionation for Antarctica and Greenland sites, *J. Geophys. Res. Atmos.*, 108(D24), n/a-n/a, doi:10.1029/2002JD003319, 2003.
 25
- Grootes, P. M. and Stuiver, M.: Oxygen 18/16 variability in Greenland snow and ice with 10-3- to 105-year time resolution, *J. Geophys. Res. Ocean.*, 102(C12), 26455–26470, doi:10.1029/97JC00880, 1997.

- Grootes, P. M. and Stuiver, M.: GISP2 Oxygen Isotope Data, [online] Available from: <https://doi.org/10.1594/PANGAEA.56094>, 1999.
- Grootes, P. M., Stuiver, M., White, J. W. C., Johnsen, S. and Jouzel, J.: Comparison of oxygen isotope records from the GISP2 and GRIP Greenland ice cores, *Nature*, 366(6455), 552–554, doi:10.1038/366552a0, 1993.
- 5 Kobashi, T., Severinghaus, J. P. and Kawamura, K.: Argon and nitrogen isotopes of trapped air in the GISP2 ice core during the Holocene epoch (0-11,500 B.P.): Methodology and implications for gas loss processes, *Geochim. Cosmochim. Acta*, 72(19), 4675–4686, doi:10.1016/j.gca.2008.07.006, 2008.
- Kobashi, T., Menviel, L., Jeltsch-Thömmes, A., Vinther, B. M., Box, J. E., Muscheler, R., Nakaegawa, T., Pfister, P. L., Döring, M., Leuenberger, M., Wanner, H. and Ohmura, A.: Volcanic influence on centennial to millennial
10 Holocene Greenland temperature change, *Sci. Rep.*, 7(1), 1441, doi:10.1038/s41598-017-01451-7, 2017.
- Lagarias, J. C., Reeds, J. A., Wright, M. H. and Wright, P. E.: Convergence Properties of the Nelder--Mead Simplex Method in Low Dimensions, *SIAM J. Optim.*, 9(1), 112–147, doi:10.1137/S1052623496303470, 1998.
- Meese, D. A., Alley, R. B., Flacco, R. J., Germani, M. S., Gow, A. J., Grootes, P. M., Illing, M., Mayewski, P. A., Morrison, M. C., Ram, M., Taylor, K., Yang, Q. and Zielinski, G. A.: Preliminary depth-age scale of the GISP2
15 ice core. [online] Available from: <https://scholar.google.ch/scholar?q=Meese%2C+D.A.%2C+R.B.+Alley%2C+R.J.+Fiacco%2C+M.S.+Germani%2C+A.J.+Gow%2C+P.M.+Grootes%2C+M.+Illing%2C+P.A.+Mayewski%2C+M.C.+Morrison%2C+M.+Ram%2C+K.C.+Taylor%2C+Q.+Yang%2C+and+G.A.+Zielinski.+1994.+Preliminary+depth-ag> (Accessed 21 March 2017), 1994.
- 20 Schwander, J., Sowers, T., Barnola, J. M., Blunier, T., Fuchs, A. and Malaizé, B.: Age scale of the air in the summit ice: Implication for glacial-interglacial temperature change, *J. Geophys. Res.*, 102(D16), 19483–19493, doi:10.1029/97JD01309, 1997.
- Steig, E. J., Grootes, P. M. and Stuiver, M.: Seasonal precipitation timing and ice core records, *Science* (80-.), 266(5192), 1885–1886, doi:10.1126/science.266.5192.1885, 1994.
- 25 Stuiver, M., Grootes, P. M. and Braziunas, T. F.: The GISP2 $\delta^{18}\text{O}$ Climate Record of the Past 16,500 Years and the Role of the Sun, Ocean, and Volcanoes, *Quat. Res.*, 44(3), 341–354, doi:10.1006/qres.1995.1079, 1995.